THE MAGNETO-OPTICAL FILTER

II. *Velocity Field Measurements*

A. CACCIANI and M. FOFI

Osservatorio Astronomico di Roma, Italy

(Received 27 March; in revised form 15 June, 1978)

Abstract. In this paper we describe a filter which utilizes magneto-optical effects for velocity fields measurements. The working principle of the instrument is described and its transmission profiles are given. Velocitygrams are shown of the five minutes oscillations (FMO) and the results compared with the expected (theoretical) signal from the instrument. We found a V_{rms} of 400 m s^{-1} for the FMO.

1. Introduction

It is very important for many problems that measurements of line shifts on the Sun are related to an absolute and steady zero level. The gravitational red shift, the oscillations of the whole Sun as a star and the downward motions in plage regions are examples of such problems. Moreover the concurrence of many causes of line shifts and their intricate spatial structure constitute the necessity for an instrument that, besides providing an absolute zero level, also visualizes the studied phenomenon as a filtergram. For this reason we have studied the properties of our magneto-optical filter (Agnelli *et al.*, 1975, Paper I) for obtaining velocitygrams. Indeed the filter seems very suitable for such a purpose because it establishes an absolute zero reference level.

The filter of Paper I can be improved by adding to it a second absorption cell embedded in a magnetic field. Among the various kinds of possible arrangements we will describe in this paper just a particular solution allowing, to a certain extent, the tuning of the transmission profile even if the magnetic field is constant and moderately strong (1.5×10^3 G).

The purpose of this paper is to describe in some detail the filter technique based on magneto-optical effects.

In Section 2 the working principle and the transmitted profiles will be shown. In Section 3 we will give the calibration curves for solar Doppler shifts. In Section 4 we will compare them with observations.

2. The Instrument

Figure 1 shows the scheme of the instrument.

The basic characteristics of the cell C are:

(a) It changes the circular polarization of the incoming light behind CP into linear polarization with orthogonal directions in the opposite wings of the solar line (the

Solar Physics **59** (1978) 179–189.

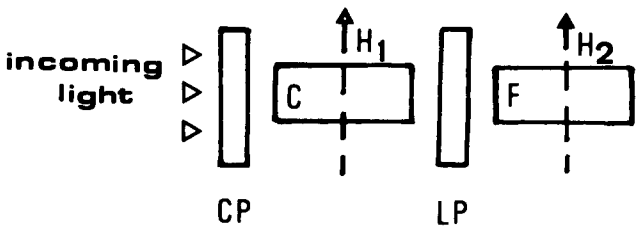

Fig. 1. *CP* is a circular polarizer, *C* is an absorption cell filled with Na vapour embedded in a magnetic field H_1. The magnetic azimuth forms an angle of 45° with the linear polarizer *LP*. *F* can be the filter of Paper I or a filter with a transverse magnetic field H_2 (parallel to H_1).

Stokes parameter V is changed into $+Q$ in the red wing and into $-Q$ in the violet one or viceversa);

(b) it provides a strong absorption in the line core.

In order to obtain the transmission profiles we use the Jones matricial calculus: each optical element in Figure 1 corresponds to a matrix operating on the state vector of the incoming light, and the output intensity I_{out} is given by square modulus of the vector

$$F \times LP \times C \times CP = \frac{F}{2}\begin{vmatrix} 1 & 1 \\ 1 & 1 \end{vmatrix} \times \begin{vmatrix} e^{i\varphi_\pi - \tau_\pi} & 0 \\ 0 & e^{i\varphi_\sigma - \tau_\sigma} \end{vmatrix} \times \frac{1}{\sqrt{2}}\left\{ \begin{vmatrix} 0 \\ 1 \end{vmatrix} \pm i \begin{vmatrix} 1 \\ 0 \end{vmatrix} \right\}, \quad (1)$$

where the circular polarization given by $CP^{\pm}$ has been split into two state vectors corresponding to linear polarizations having a phase difference equal to $\pm \pi/2$ (see the factor $i = \exp(\pm i\pi/2)$; the + or − sign is depending on the handedness of the circular polarization, lefthanded or righthanded); φ_π and φ_σ are the absolute phase delay in the Zeeman pattern; τ_π and τ_σ are the corresponding optical depths of the vapour inside the cell C; finally F is the transmission profile of the filter *F*. φ_π, φ_σ, τ_π and τ_σ are the functions of λ (see Paper I).

By developing the expression (1) we have:

$$I^{\pm}_{\text{out}} = F \times \tfrac{1}{2} \times [e^{-2\tau_\sigma} + e^{-2\tau_\pi} \pm e^{-\tau} \sin \delta], \quad (2)$$

where $\tau = \tau_\pi + \tau_\sigma$ and $\delta = \varphi_\sigma - \varphi_\pi$ is the relative phase delay between π and σ components.

In this expression the crucial term is $\pm e^{-\tau} \sin \delta$.

Two very important properties should be pointed out about it. First, δ changes its sign for the opposite wings of the line (see Figure 2) so that in the Equation (2) it gives rise to a maximum in one wing (depending on the sign $CP^{\pm}$) and a minimum in the opposite one (Figure 4b, c): the Doppler signal is therefore obtained by changing CP^{+} into CP^{-} and forming the difference $I^{+}_{\text{out}} - I^{-}_{\text{out}} = Fe^{-\tau} \sin \delta$ (see Figures 3 and 4). Second, δ is a function of the vapour optical depth inside the cell so that it also provides a suitable way for a slight tuning of the position in λ of the transmission maximum (Figure 3b).

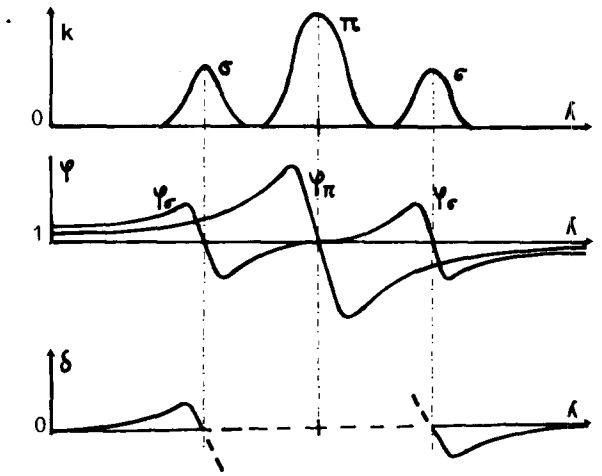

Fig. 2. K is the absorption coefficient for a normal Zeeman split triplet. φ_π and φ_σ are the absolute phase delays and the relative phase delay is $\delta = \varphi_\sigma - \varphi_\pi$.

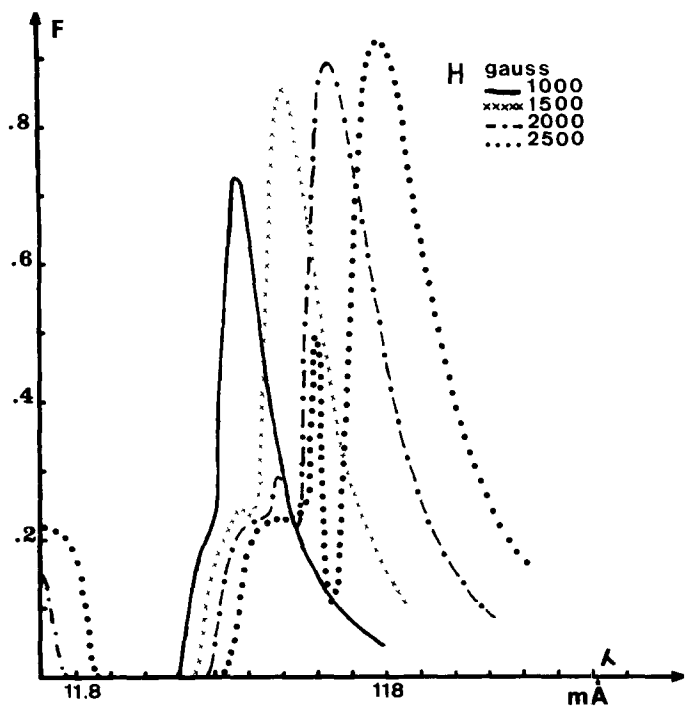

Fig. 3a. Behaviour of the function F for various values of the magnetic field.

Note further that the transparency of the cell C at the maximum can be very high, near 100%; as it is caused by the Macaluso–Corbino effect (i.e. the Faraday rotation near a Zeeman split absorption line) quite far from the absorbing region. The

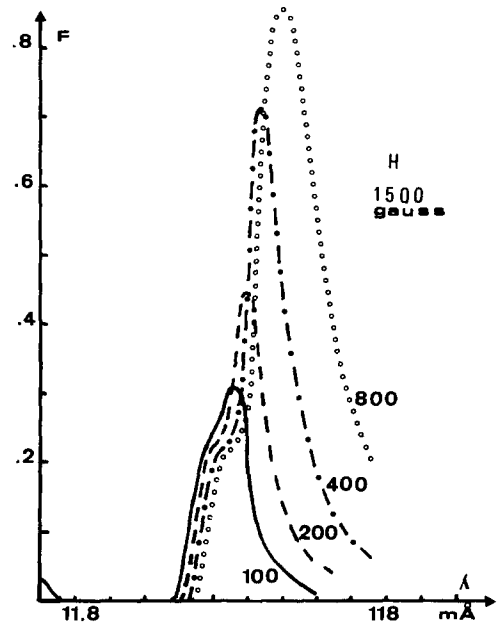

Fig. 3b. Behaviour of the function F for various values of the vapour optical depth τ. —— $\tau = 100$, – – – $\tau = 200$, – · – $\tau = 400$, ° ° ° ° ° $\tau = 800$.

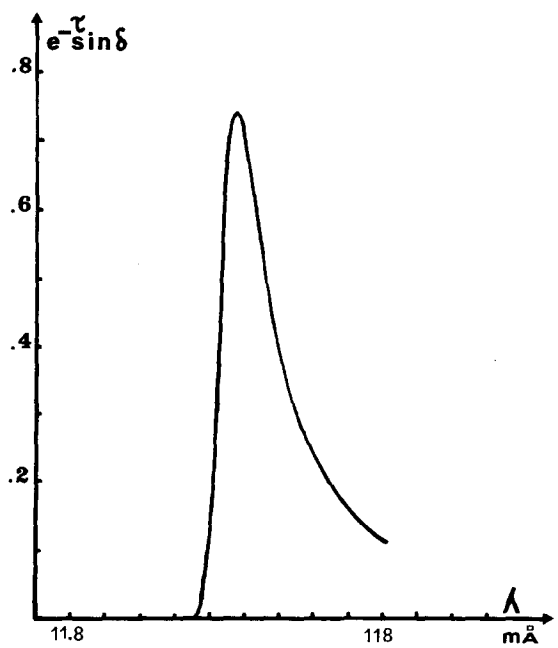

Fig. 3c. Behaviour of the function $e^{-\tau} \sin \delta$. Because of the property of δ (see text and Figure 2) it is antisymmetric and its integrate signal is a measure of the input line shift.

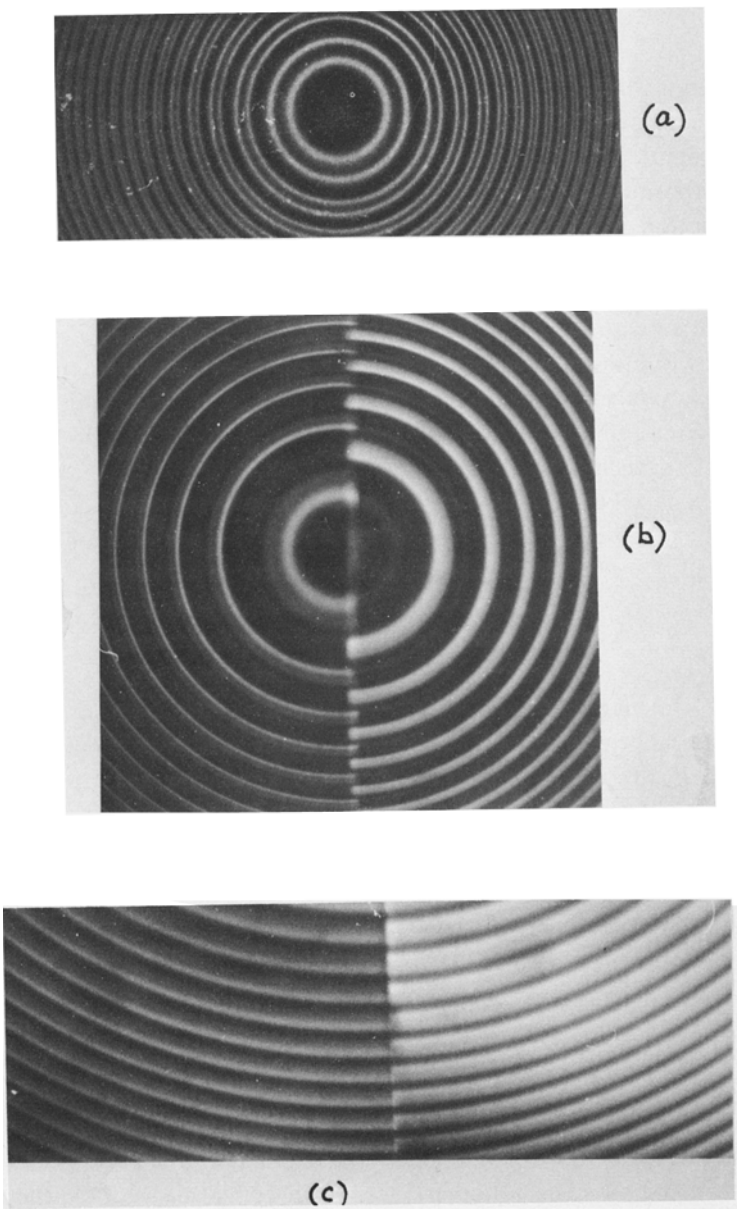

Fig. 4a–c. Spectra taken with a Fabry–Perot Interferometer: spectral range = 200 mÅ. Input: Na lamp. (a) transmission of the filter *F*. (b) transmission after *LP* of Figure 1. Only one wing is transmitted. D_1 on the left and D_2 on the right. (c) The same as (b) for D_2 alone. *CP* is positive on the left and negative on the right: the transmitted wing is consequently changed.

filter F is designed in such a way as to have its transmission maxima tuned with those produced by the cell C. If the filter F uses a transverse magnetic field we have:

$$F = e^{-2\tau_\pi^*} + e^{-2\tau_\sigma^*} - 2e^{-\tau^*} \cos \delta , \tag{3}$$

where * means that the quantities are referring to the filter F instead of the cell C.

In Figures 3a and 3b F is plotted and in Figure 3c the term $e^{-\tau} \sin \delta$ is shown.

In our computations, which refer to an homogeneous magnetic field H_1, an unwanted transmission band at $\lambda = 0$ appears. However it is possible to cut it off by pure absorption inside the cell C. In fact the spatial configuration of H_1 and distribution of sodium vapour strongly affect the actual working properties of the instrument. This has been tested both theoretically and experimentally and in Figure 4 spectra taken with a Fabry-Perot interferometer are given.

Let us now suppose that CP is removed and that we are observing a solar region with a longitudinal magnetic field. The polarization of the incoming light then arises from the Zeeman effect and it is restricted to the line wings with opposite signs on the red and violet side. In this case the antisymmetry of the term $\pm e^{-\tau} \sin \delta$ allows both polarized wings to be transmitted or absorbed according to the direction of the solar magnetic field. Therefore the instrument is also suitable for magnetic field measurement.

3. Application to Solar Velocity Field

As a test for the magneto-optical filter, we have measured the velocity of the FMO.

In order to calibrate the filter, it is necessary to calculate the signal expected due to a given velocity at various positions of the solar disk. This calculation (calibration) is possible because: (i) the magneto-optical filter gives us an absolute and stable zero reference level through its own absorption lines, and (ii) the solar profiles of the sodium D lines are very well studied both observationally and theoretically for different μ.

By photographic subtraction of two filtergrams we obtain:

$$\Delta D = \gamma(\log e)\, \Delta I / I_\lambda , \tag{4}$$

where ΔD is the density excursion of an observed point from the mean value; I_λ is the residual light intensity on the line profile at wavelength λ referred to the zero reference of the filter; finally ΔI is the intensity variation caused by the FMO.

We computed $\Delta I / I_\lambda$ as a function of the Doppler shift for $|v| \leq 1 \text{ km s}^{-1}$ (i.e. $\Delta\lambda \leq 20$ mÅ) and for solar latitudes $|L| \leq 30°$. In doing this we took due account of (Howard and Harvey, 1970):

(a) Solar differential rotation: for the sodium D lines, at the equator and at the limbs, it amounts to ± 37.93 mÅ.

(b) Earth rotation: during equinox at the sunrise and sunset it amounts to ± 6.32 mÅ for our latitude 43° 45′ 04″.

(c) Gravitational red shift: equal to 12.72 mÅ.

We ignored the ellipticity of the Earth orbit and the limb shift of the solar lines. The latter effect is found practically inexistent for the Na D lines (Hart, 1974). We made use of the Waddel profiles for the solar lines, μ ranging from 0.3 to 1.0 (Waddel, 1962), and of our results of Paper I for the transparency profiles of the magneto-optical filter.

Figure 5 shows an example of the calibration curves for the solar equator at noon. The strong E–W asymmetry in the curves is caused by the effect (c) and is further enhanced at sunset time by the effect (b).

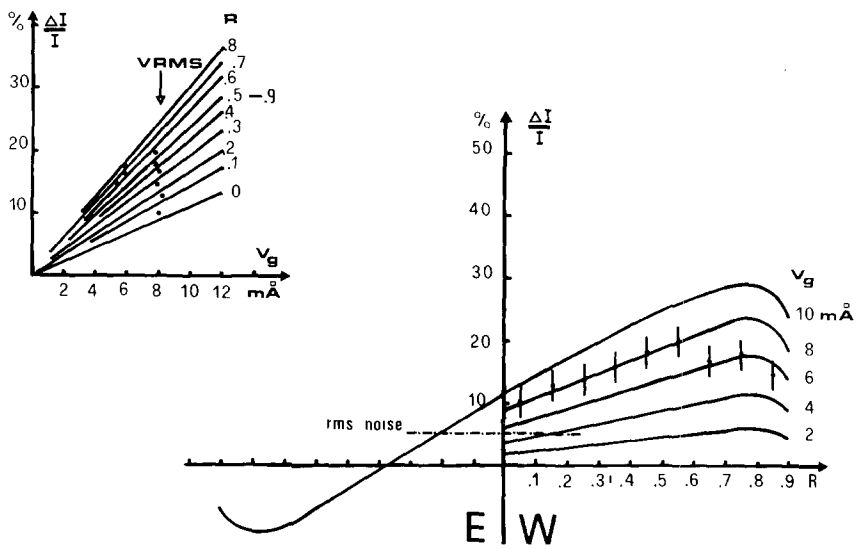

Fig. 5. Calibration curves with experimental points (Equation (5a)) of the filter of Paper I. The total error on the experimental points has been assumed equal to the noise rms. R is the distance from the center of the disk.

4. Observations

The east and the west part of the Sun, as they appear through the filter F, are shown in Figure 6. The useful aperture of the filter was 20 mm and the angular field at present is about 10°. With a telescope aperture $f/15$ the exposure time was about $\frac{1}{8}$ s. This can be lowered considerably by increasing the magnetic field.

The mottling, typical for spectroheliograms of metallic lines, is more pronounced in the west side. This fact corresponds to the well known behaviour of the mottling visibility along the line profile (D'Azambuja, 1930): the tuning, in our case, is given by the solar rotation. By analysing the photographically subtracted pairs of filtergrams of a time series we found that the highest contrast occurs for a lag of 2.5 min. This result is expected, i.e. the mottling in a filtergram is caused also by FMO. The original filtergrams were recorded using the PDS microdensitometer of Naples Observatory and the data stored on magnetic tape for digital analysis.

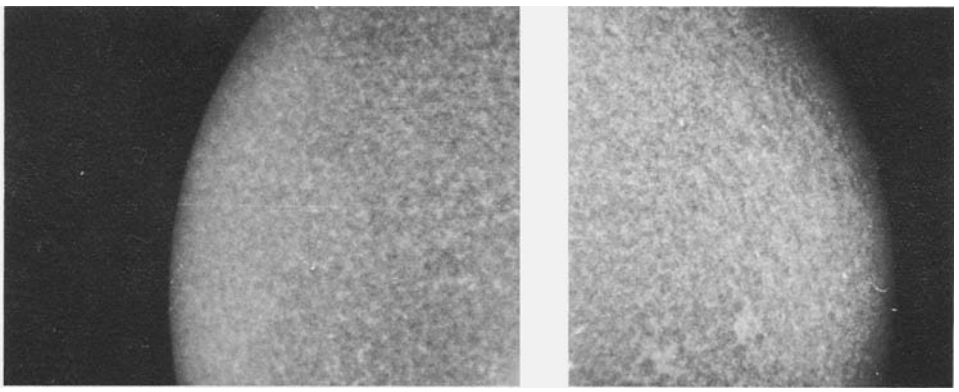

Fig. 6. Comparison of the east and west part of a filtergram through the magneto-optical filter. Note the enhanced mottling in the western hemisphere.

Figure 7 shows a low resolution fulldisk photographic subtraction and in Figure 8 a region with 2 arc sec resolution is shown.

Oscillations are well visible on the west side and the local contrast is slowly decreasing towards the east side. This behaviour has been discussed in Section 3.

In order to compare theory and observation we plotted the quantities given in Equations (5a) and (5b):

$$\left(\frac{\Delta I}{I}\right)_{\text{rms}} = \frac{1}{0.43\gamma}\sqrt{(D-D_0)^2_{\text{rms}} - N^2}\,, \tag{5a}$$

where D_0 is the local mean photographic density calculated by fitting a second order polynomial to each densitometer trace. We used, for this purpose, 10 traces near the equator. N is the noise rms density fluctuation given by direct measurement in the east part of the velocitygram or by the granularity of the film (Brandt and Nesis, 1973). The experimental points reproduce the behaviour of the curves of Figure 5 and fit with $v_{\text{rms}} \approx 8$ mÅ $= 400$ m s^{-1}. The last three points of the particular velocitygram we used suggest $v_{\text{rms}} \approx 6$ mÅ rather than 8 mÅ. This figure however should be taken with caution because of the great uncertainty on the accuracy of the photographic processing and, in particular, on the factor γ. (A better estimate of v_{rms} will be achieved when our program of photo-electric image detection through a TV camera and CCD diode array will be completed.)

$$C_\rho = 1 - \int_{D_0-1.5N}^{D_0+1.5N} P(D)\,\mathrm{d}D\,, \tag{5b}$$

where $P(D)$ is the local density distribution function in the velocitygram. C_ρ better represents the visual contrast behaviour: in fact in a given region of the Sun containing many oscillating elements, the mean position of which is determined by the heliographic vector $\boldsymbol{\rho}$, the overall visual contrast $C(\boldsymbol{\rho})$ is given by the probability

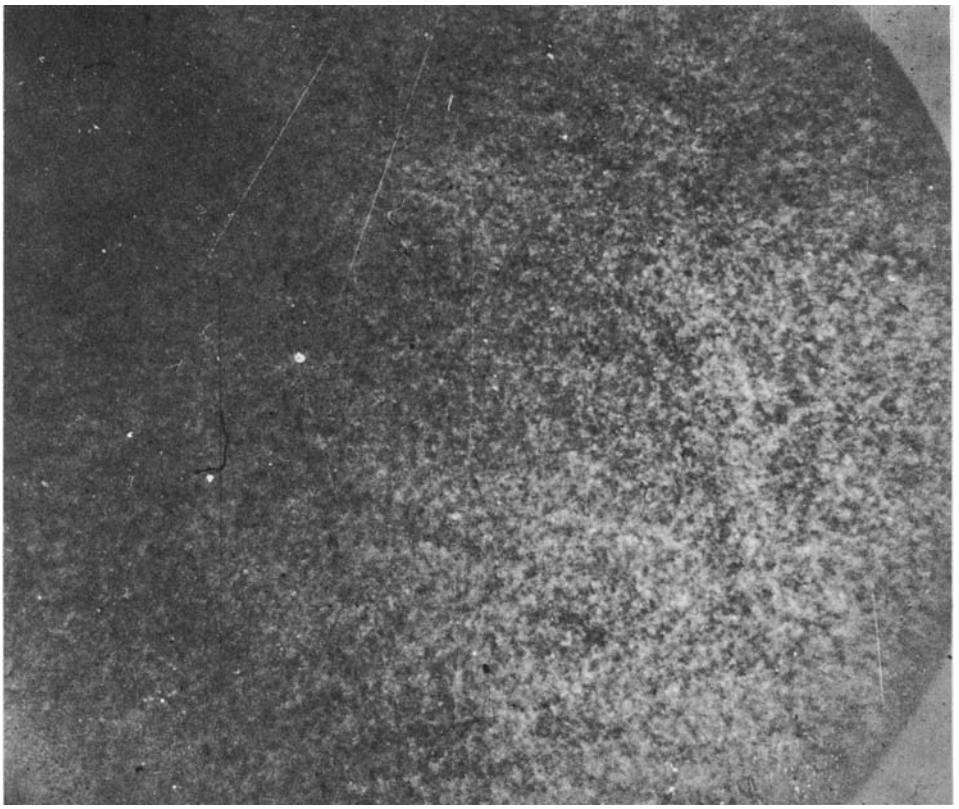

Fig. 7. Full disk photographic subtraction between filtergrams with a time delay of 2.5 min. Note that the oscillatory field is visible only on the western hemisphere.

of finding pairs of points with velocities quite different from one another, for example more different than three times the noise rms fluctuation N; that is, if $P(D)$ is the probability to find a density D in the first point of a pair and

$$1-\int_{D-1.5N}^{D+1.5N} P(D)\,\mathrm{d}D$$

is the probability that the second point has a density D' such as $|D'-D| \geqslant 1.5N$, we have

$$C_\rho = \int_0^\infty P(D)\left[1-\int_{D-1.5N}^{D+1.5N} P(D')\,\mathrm{d}D'\right]\mathrm{d}D.$$

For the second mean theorem it is also

$$C_\rho = 1-\int_{D_m-1.5N}^{D_m+1.5N} P(D)\,\mathrm{d}D\,,$$

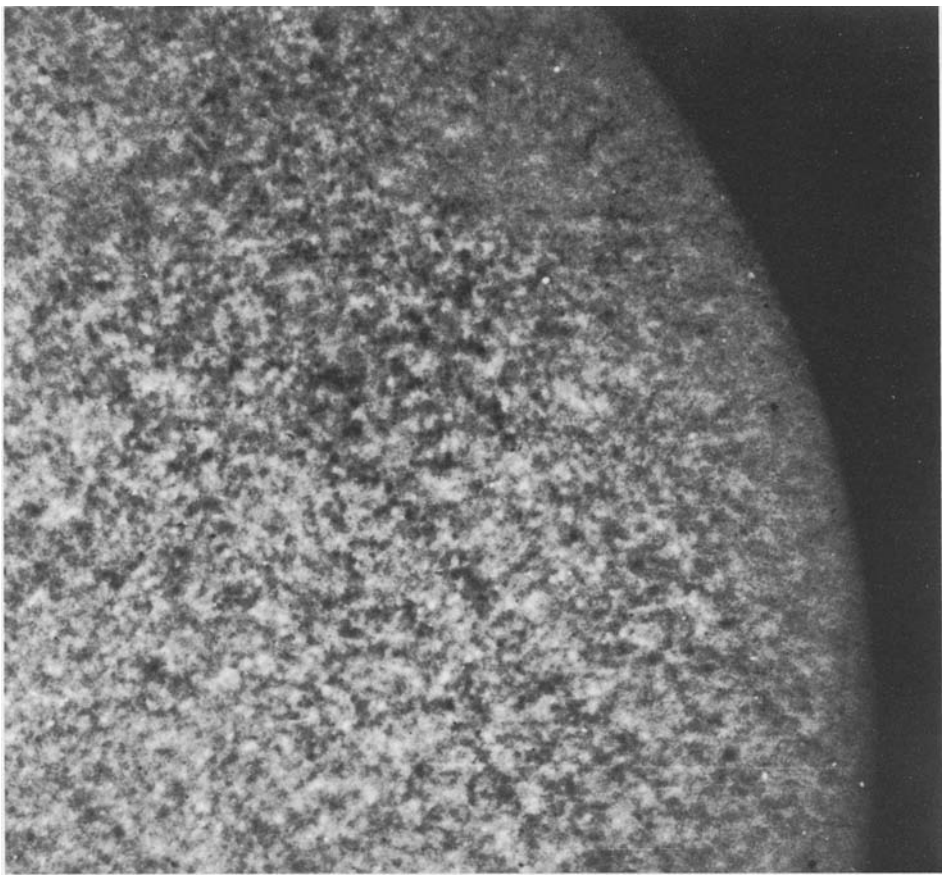

Fig. 8. Portion of a velocitygram with 2 arc sec resolution.

where D_m is function of ρ quite near to D_0. Therefore expression (5b) follows for C_ρ and it is given by the number of points with $D > (D_0 + 1.5N)$. In Figure 9 it is shown the behaviour of C_ρ along the solar equator on the west side.

5. Summary and Conclusion

We have shown and analyzed in detail the working principle of an instrument which utilizes the magneto-optical filter of Paper I for the measurement and the visualization of the solar velocity field. We have then tested the filter by comparing its expected sensitivity for line shifts with densitometric tracings of observed velocitygrams. For the computations we have used the profile of the solar Na D lines by Waddel and the transparency profiles of the filter given in Paper I. Such a study gives the necessary calibration of the instrument. At present we are collecting further observations of FMO. The results of these observations will be given in due time.

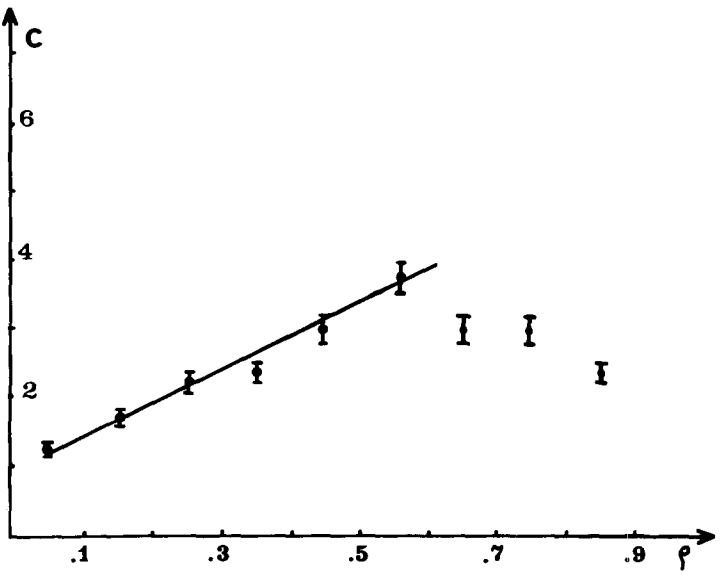

Fig. 9. The behaviour of C_ρ (arbitrary units) is very similar to the experimental points of Figure 5.

Acknowledgements

We are grateful to Dr R. Habel and Mr S. Viligiardi for the practical realization of the sodium cells, to Prof. M. Rigutti and Mrs A. M. Caccin for the PDS scanner of Napoli Observatory and to the Director and the Staff of the Arcetri observatory for help and hospitality. We also thank Mr F. Alimandi, Rome Observatory, for the photographic processing.

References

Agnelli, G., Cacciani, A., and Fofi, M.: 1975, *Solar Phys.* **44**, 509.
Brandt, P. N. and Nesis, A.: 1973, *Solar Phys.* **31**, 75.
D'Azambuja, L.: 1930, *Ann. Obs. Meudon* **8**, fasc. 2.
Hart, M. H.: 1974, *Astrophys. J.* **187**, 393.
Howard, R. and Harvey, J.: 1970, *Solar Phys.* **12**, 23.
Waddel, J.: 1962, *Astrophys. J.* **136**, 223.